Research Square

Preprints are preliminary reports that have not undergone peer review.
They should not be considered conclusive, used to inform clinical practice,
or referenced by the media as validated information.

Mechanistic insights into radiosensitization by high atomic number nanoparticles during 177Lu targeted radionuclide therapy using Monte Carlo simulation

Fatemeh mahdavi
Tehran University of Medical Sciences
Amir reza Jalilian
International Atomic Energy Agency (IAEA), Vienna, Austria
Fariba Esmaili
Tehran University of Medical Sciences, Tehran, Iran
Sharmin Kharrazi
Tehran University of Medical Sciences, Tehran, Iran
Parham Geramifar
pgeramifar@gmail.com

Tehran University of Medical Sciences

Research Article

Keywords: 177Lu, high-Z nanoparticles, Geant4-DNA, Monte Carlo simulation, dose enhancement factor, targeted radionuclide therapy, radiosensitization, DNA damage, secondary electrons, polyethylene glycol

Posted Date: November 12th, 2026

DOI: https://doi.org/10.21203/rs.3.rs-11335859/v1

License: This work is licensed under a Creative Commons Attribution 4.0 International License.
Read Full License

Additional Declarations: No competing interests reported.

Mechanistic insights into radiosensitization by high atomic number nanoparticles during 177Lu targeted radionuclide therapy using Monte Carlo simulation

Fatemeh Mahdavi[1,2], Amir Reza Jalilian[3], Fariba Esmaili[2], Sharmin Kharazi[2*], Parham Geramifar[1*]

[1].Research Center for Nuclear Medicine, Tehran University of Medical Sciences, Tehran, Iran
[2]Department of Medical Nanotechnology, School of Advanced Technologies in Medicine, Tehran University of Medical Sciences, Tehran, Iran
[3]International Atomic Energy Agency (IAEA), Vienna, Austria

*Author to whom correspondence should be addressed:
Correspond: pgeramifar@gmail.com
Co-Correspond: sh-kharrazi@tums.ac.ir

Abstract

Background: High-Z nanoparticles have emerged as promising radiosensitizers for targeted radionuclide therapy by increasing nanoscale energy deposition and secondary electron production. Although Monte Carlo studies have extensively investigated photon-induced radiosensitization, the mechanisms underlying nanoparticle-enhanced beta-emitting radionuclide therapy remain insufficiently understood. This study evaluated the influence of nanoparticle composition and surrounding medium on radiation interactions, reactive species generation, and DNA damage during 177Lu irradiation.

Objective: To investigate the dosimetry and radiobiological effects of high-Z nanoparticles combined with the beta-emitting radionuclide 177Lu using Geant4-DNA Monte Carlo simulations.

Methods: Two complementary simulation models were developed. First, 25 nm nanoparticles (Au, Ag, Pt, Ta, Pd, Gd, Fe, Ti, and their oxides) were simulated in spherical water and polyethylene glycol (PEG)-based phantoms to evaluate dose enhancement factors (DEFs), secondary particle production, and radiation interactions using Livermore, Penelope, and Geant4-DNA physics models. Second, a fibroblast cell model containing distributed nanoparticles and intracellular 177Lu sources was used to assess reactive species production and radiation-induced DNA damage, including single- and double-strand breaks.

Results: High-Z nanoparticles significantly increased local energy deposition and secondary electron production compared with nanoparticle-free media. Tantalum nanoparticles exhibited the highest dose enhancement, followed by

platinum and gold. Dose enhancement reached approximately 1200% (DEF ≈ 13) in the immediate vicinity of the nanoparticle surface and gradually decreased with increasing distance. PEG-based media produced moderately higher energy deposition than water. Nanoparticle incorporation also increased reactive species generation and enhanced both direct and hydroxyl radical-mediated indirect DNA damage. Penelope and Livermore models showed consistent material-dependent trends with only minor differences in secondary particle yields.

Conclusion: High-Z nanoparticles substantially enhance 177Lu-induced radiation effects by increasing local dose deposition, secondary electron production, reactive species generation, and simulated DNA damage. Tantalum demonstrated the greatest radio sensitizing potential, highlighting its promise as a nanoparticle enhancer for targeted radionuclide therapy.

Keywords: 177Lu; high-Z nanoparticles; Geant4-DNA; Monte Carlo simulation; dose enhancement factor; targeted radionuclide therapy; radiosensitization; DNA damage; secondary electrons; polyethylene glycol.

Introduction

Targeted radionuclide therapy (TRT) has become an important treatment modality for a variety of malignancies by selectively delivering ionizing radiation to tumor tissues through radiopharmaceuticals. Among therapeutic radionuclides, lutetium-177 (177Lu) has gained widespread clinical acceptance owing to its favorable physical and radiobiological properties, including medium-energy β-particle emissions (maximum energy ≈497 keV), a relatively short tissue penetration range (approximately 2 mm), and low-energy γ emissions that enable post-treatment imaging and dosimetric assessment. These characteristics have led to the successful clinical application of 177Lu-based therapies, particularly in patients with neuroendocrine tumors and metastatic prostate cancer. However, despite these advances, therapeutic outcomes remain suboptimal in a proportion of patients because of heterogeneous dose distribution within tumors, limited dose escalation, and the intrinsic radioresistance of certain cancer cells. Consequently, strategies capable of increasing radiation effectiveness at the cellular and subcellular levels continue to attract considerable interest.[1]

High-atomic-number (high-Z) nanoparticles have been extensively investigated as radiosensitizers because of their ability to increase local radiation interactions and enhance secondary electron production. Nanomaterials such as gold,

platinum, and tantalum possess favorable physical characteristics that can promote localized energy deposition following irradiation. While the radiosensitizing effects of high-Z nanoparticles have been widely explored under kilovoltage X-ray irradiation, their role in targeted radionuclide therapy with β-emitting radionuclides has received considerably less attention.[2]

Unlike photons, β particles deposit energy primarily through direct ionization and excitation of matter rather than photoelectric interactions. As a result, the mechanisms underlying nanoparticle-mediated enhancement during β irradiation differ from those observed in photon-based radiotherapy. In β-emitter therapy, radiation enhancement is thought to arise mainly from increased production of low-energy secondary electrons, localized energy deposition, and subsequent amplification of radiation-induced chemical reactions that contribute to biological damage.[3]

The surrounding biological environment is another important factor influencing nanoparticle-mediated radiation effects. Although most Monte Carlo simulations are performed in pure water, intracellular and extracellular environments contain biomolecules and polymers that modify electron transport, radical diffusion, and radiation chemistry. Polyethylene glycol (PEG), a biocompatible polymer widely used as a nanoparticle coating to prolong circulation time and reduce immunogenicity, represents a biologically relevant medium with physicochemical properties that differ from those of water and may therefore influence radiation interactions and reactive species production.[4]

Monte Carlo track-structure simulations provide a powerful framework for investigating radiation effects across physical, chemical, and biological scales. In particular, the Geant4-DNA extension enables nanometer-scale simulation of low-energy particle transport, water radiolysis, reactive species generation, and radiation-induced DNA damage, making it a valuable tool for mechanistic studies of nanoparticle-assisted radionuclide therapy. [5,6]

Despite increasing interest in nanoparticle-mediated radiosensitization, several important questions remain unresolved for 177Lu-based targeted radionuclide therapy. Previous studies have focused predominantly on gold nanoparticles under photon irradiation, whereas systematic comparisons of multiple high-Z metals and their corresponding oxides during β-particle irradiation remain scarce. Moreover, the influence of different electromagnetic physics models, biologically relevant surrounding media, and the relationship between physical dose enhancement, radiation chemistry, and DNA damage have not been comprehensively investigated.

To address these knowledge gaps, the present study systematically evaluated the physical, chemical, and biological effects of sixteen high-Z nanoparticle materials, including pure metals and their corresponding oxides, during 177Lu β irradiation using Geant4-DNA Monte Carlo simulations. Simulations were performed in both water and polyethylene glycol (PEG)-based media to investigate dose enhancement, secondary particle production, reactive species generation, and radiation-induced DNA damage. In addition, the performance of the Livermore and Penelope electromagnetic physics models was compared under identical simulation conditions to assess the consistency and robustness of the predicted nanoparticle enhancement effects. [7,8]

2. Methods

This study was conducted as a comprehensive Monte Carlo investigation to evaluate the physical, chemical, and biological effects of high-Z nanoparticles during 177Lu-based targeted radionuclide therapy. Simulations were designed to quantify nanoparticle-induced dose enhancement, secondary particle production, radiation chemistry, and DNA damage using both simplified single-nanoparticle geometries and a biologically realistic fibroblast cell model. The overall simulation workflow consisted of sequential physical, physicochemical, chemical, and biological stages implemented within the Geant4 framework.

2.1 Simulation Framework

All simulations were performed using the Geant4 Monte Carlo toolkit (version 11.0.1) together with the Geant4-DNA extension for track-structure simulation of low-energy charged particles and radiation-induced water radiolysis. Two electromagnetic physics models, Livermore and Penelope, were independently implemented under identical simulation conditions to evaluate the influence of physics model selection on nanoparticle-mediated radiation enhancement. Within nanometer-scale regions surrounding the nanoparticles, Geant4-DNA Option4 track-structure physics was activated to accurately simulate low-energy electron transport and interaction processes.

Two complementary simulation configurations were developed. The first consisted of an isolated single-nanoparticle model designed to evaluate dose enhancement, secondary particle production, and radiation interaction mechanisms. The second employed a realistic fibroblast cell geometry containing intracellular nanoparticles and distributed 177Lu

sources to investigate energy deposition, reactive species generation, and radiation-induced DNA damage under biologically relevant conditions [9,10].

2.2 Single Nanoparticle Geometry

The physical model consisted of a spherical nanoparticle with a radius of 25 nm positioned at the center of a spherical phantom with a radius of 1 mm. Simulations were performed using two surrounding media: liquid water (density = 1.0 g/cm³) and polyethylene glycol (PEG) polymer (density = 1.125 g/cm³), allowing evaluation of the influence of the local chemical environment on radiation transport and dose deposition. The schematic representation of the single-nanoparticle simulation geometry is shown in Figure 1.

Sixteen nanoparticle materials were investigated, including eight pure metals (Au, Ag, Pt, Ta, Pd, Gd, Fe, and Ti) together with their corresponding oxides (Au_2O_3, Ag_2O, PtO_2, Ta_2O_5, PdO, Gd_2O_3, Fe_3O_4, and TiO_2). Simulations of homogeneous water and PEG media without nanoparticles were performed as reference conditions for dose enhancement calculations.

A spherical water region immediately surrounding each nanoparticle was defined as a dedicated Geant4-DNA track-structure region, whereas the remaining phantom volume was simulated using either the Livermore or Penelope electromagnetic physics model. Radial dose deposition and secondary particle distributions were quantified using concentric spherical scoring shells extending from the nanoparticle surface to the outer boundary of the phantom [11,12]. The radial scoring geometry is illustrated in Figure 2.

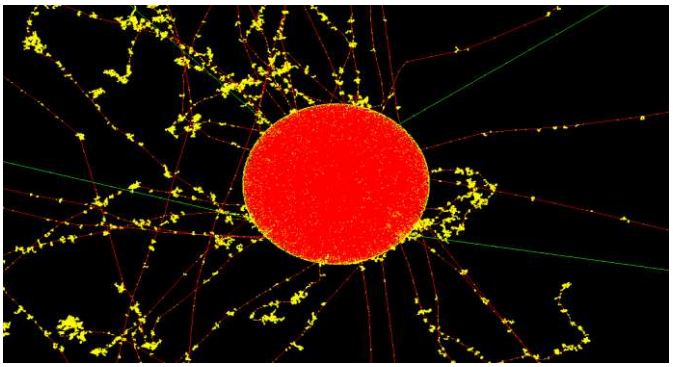


Figure 1. Schematic representation of the single-nanoparticle simulation geometry. A spherical nanoparticle (radius = 25 nm) was positioned at the center of a spherical phantom filled with either water or polyethylene glycol (PEG) medium.

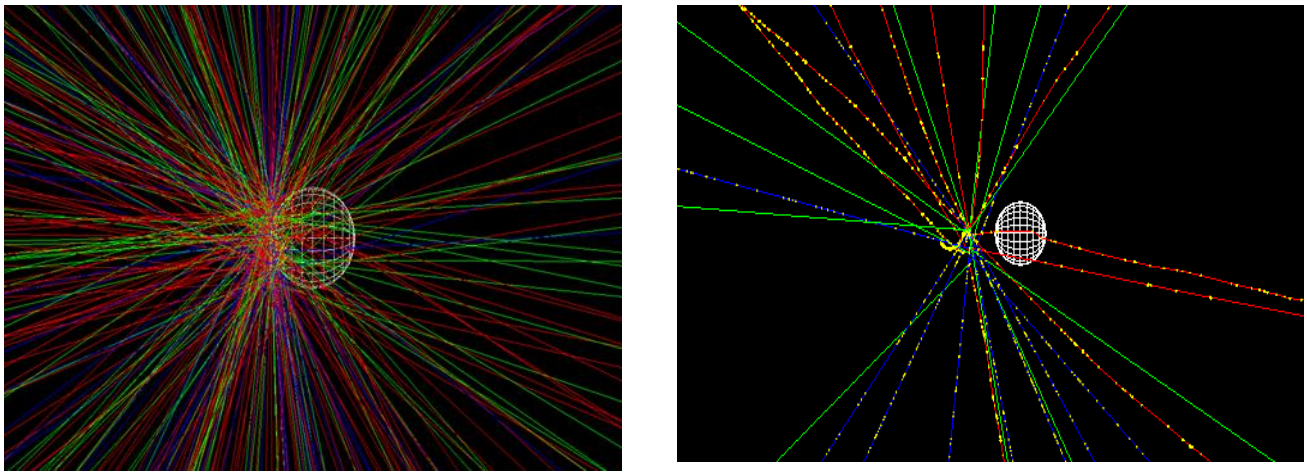


Figure 2. Radial scoring geometry used to quantify absorbed dose and secondary particle production. One hundred concentric spherical scoring shells extended from the nanoparticle surface (25 nm) to the outer boundary of the phantom (1 mm).

2.3 Radiation Source

The 177Lu source was modeled as a β^- emitter using the Geant4 General Particle Source (GPS) module. The continuous β-particle energy spectrum, with a maximum energy of approximately 497 keV, was implemented according to the decay characteristics of 177Lu. The source was represented as a spherical volume with a radius of 25 nm and positioned on the negative *z*-axis at a distance of 25 nm from the nanoparticle surface.

Primary particles were emitted isotropically from the source volume. Depending on the simulation objective, the number of primary histories ranged from 1×10^5 for absorbed dose calculations to 2×10^9 for high-statistics analyses of secondary particle production, ensuring acceptable statistical uncertainty for all scored quantities [13].

2.4 Physics Models and Transport Parameters

Two low-energy electromagnetic physics models available in Geant4 were evaluated in this study: the Livermore and Penelope electromagnetic physics constructors. The minimum production thresholds were set to 250 eV for the Livermore model and 100 eV for the Penelope model.

To accurately describe nanoscale interactions in the vicinity of the nanoparticles, Geant4-DNA Option4 track-structure physics was activated within the dedicated nanoparticle-surrounding region. A maximum transport step length of 1 nm was imposed throughout this region to improve the spatial accuracy of low-energy electron transport and energy deposition [14].

2.5 Dose Enhancement Factor (DEF)

The dose enhancement factor (DEF) was used to quantify the influence of nanoparticles on local energy deposition. DEF was calculated as the ratio of the absorbed dose in the presence of a nanoparticle to the absorbed dose obtained under identical conditions in the corresponding nanoparticle-free reference medium:

Equation (1) $$\mathrm{DEF} = \frac{D_{\mathrm{NP}}}{D_{\mathrm{Ref}}}$$

where D_{NP} and D_{Ref} represent the absorbed doses with and without nanoparticles, respectively.

Radial DEF profiles were calculated from the nanoparticle surface to a distance of approximately 10 μm to characterize the spatial distribution of nanoparticle-induced dose enhancement [15].

2.6 Secondary Particle Analysis

Secondary particle production was evaluated using a custom Geant4 stepping analysis. Only particles with a track ID greater than 1 were classified as secondary particles and included in the analysis. The scored particles included secondary electrons, photons, and positrons generated during radiation transport.

Interaction mechanisms were identified using the G4PhysicsModelCatalog framework and included ionization, Auger electron emission, characteristic X-ray production, Bremsstrahlung, and particle-induced X-ray emission (PIXE). Secondary particle yields were normalized either per primary event by dividing the total counts by the number of primary particles or per radionuclide decay using the decay characteristics of 177Lu to facilitate quantitative comparisons among different nanoparticle materials.

2.7 Full-Cell Geometry

To investigate nanoparticle-mediated radiation effects under biologically relevant conditions, a realistic fibroblast cell model was constructed. The geometry consisted of two concentric ellipsoids representing the cytoplasm (13 × 10 × 5 μm) and nucleus (11.82 × 8.52 × 3 μm), respectively. Chromatin was represented by an array of cubic domains uniformly distributed throughout the nuclear volume to enable nanoscale scoring of radiation-induced DNA damage. The Geant4-based fibroblast cell geometry, including the cytoplasm, nucleus, and chromatin domains, is illustrated in Figure 3.

Spherical nanoparticles with a radius of 25 nm and intracellular 177Lu sources were randomly distributed throughout the cytoplasmic compartment using a vector-based positioning algorithm. The nanoparticle concentration was fixed at approximately 100 ppm, and simulations were performed using 1×10^6 primary particle histories. This geometry enabled evaluation of intracellular energy deposition, reactive species generation, and nanoparticle-induced DNA damage under realistic irradiation conditions. The random intracellular distribution of nanoparticles and internalized ^{177}Lu sources is illustrated in Figure 4.

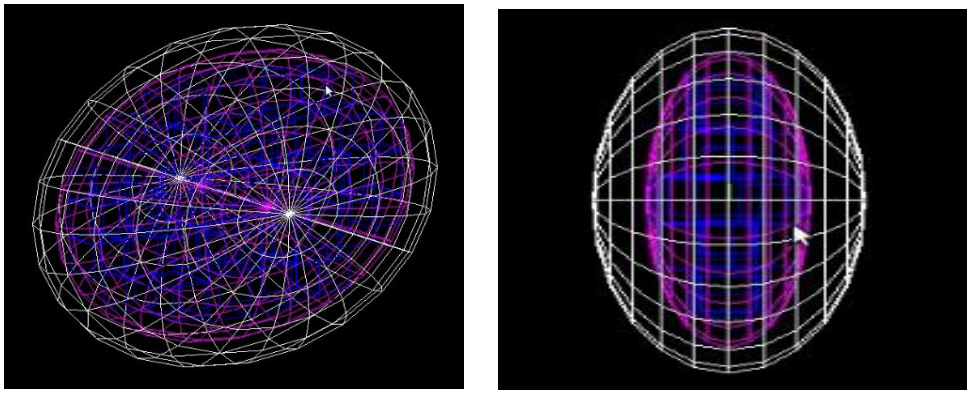


Figure 3. Geant4-based fibroblast cell model used for biological simulations, illustrating the cytoplasm, nucleus, and chromatin domains employed for DNA damage analysis.

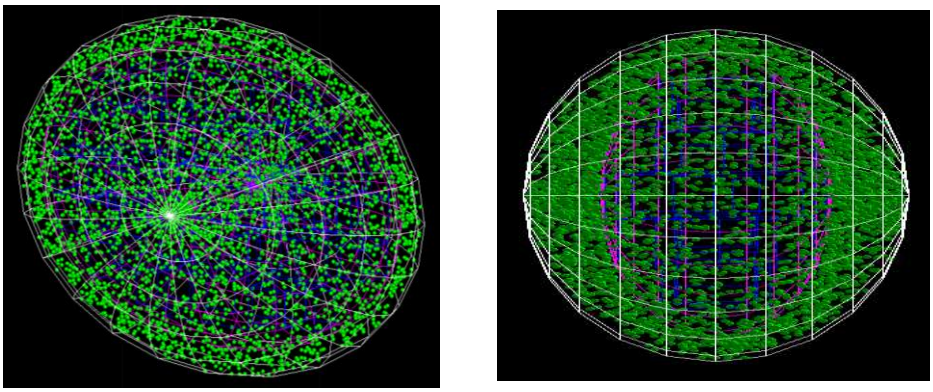


Figure 4. Simulation geometry showing the random intracellular distribution of 25 nm nanoparticles and internalized 177Lu sources within the cytoplasm of the fibroblast cell model.2.8 DNA Damage Modeling

2.8 DNA Damage Modeling

Radiation-induced DNA damage was quantified using the Geant4-DNA track-structure framework by considering both direct energy deposition and indirect damage mediated by reactive chemical species. DNA lesions were classified as single-strand breaks (SSBs) and double-strand breaks (DSBs) according to established Geant4-DNA scoring criteria [16].

A direct SSB was recorded when the energy deposited within the DNA backbone exceeded 17.5 eV. For deposited energies between 5 and 37.5 eV, the probability of strand break formation was determined using linear interpolation. A DSB was defined as two SSBs located on opposite DNA strands and separated by no more than 3.4 nm, corresponding to approximately 10 base pairs.

DNA damage was categorized into three classes:

- Direct damage, resulting from direct energy deposition by charged particles;
- Indirect damage, caused by hydroxyl radicals (•OH) generated during water radiolysis;
- Hybrid DSBs, consisting of one direct and one indirect strand break.

Only hydroxyl radicals were considered in the indirect damage calculations because they are regarded as the predominant reactive species responsible for radiation-induced DNA damage under physiological conditions [17].

2.9 Chemical Species Production and Radical Enhancement Factor (REF)

Chemical-stage simulations were performed to evaluate radiation-induced reactive species production following the physical interaction stage. Radiation chemistry calculations were implemented using the Geant4-DNA Independent Reaction Time (IRT) chemistry module (Option3), which enables simulation of radical diffusion and chemical reactions over biologically relevant timescales.

The energy spectra of secondary electrons generated during the physical stage were recorded and subsequently used as input for the chemical-stage simulations. Reactive species produced during water radiolysis were tracked, including hydrated electrons e^-_{aq}, hydroxyl radicals (•OH), hydrogen atoms (•H), hydrogen peroxide (H_2O_2), molecular hydrogen (H_2), hydronium ions (H_3O^+), hydroxide ions (OH^-), and other transient radiolytic products [18].

The chemical stage was simulated at 10 ps, 1 ns, and 1 μs, representing the formation, diffusion, and reaction phases of radiation-induced radicals. Radical production before 10 ps was not evaluated because reactive species have not yet fully formed during the preceding physicochemical stage. Chemical transport was terminated at 1 μs, consistent with the temporal range adopted in Geant4-DNA chemistry simulations.

Radical yields were quantified using concentric spherical scoring shells positioned around the nanoparticle surface with a radial spacing of 25 nm. The scoring region extended from the nanoparticle surface to a distance of 1 mm, enabling evaluation of the spatial distribution of reactive species generated by nanoparticle-enhanced β irradiation.

The G-value, defined as the number of chemical species produced per 100 eV of deposited energy, was calculated for each radical species. In addition, the Radical Enhancement Factor (REF) was determined by comparing radical yields in nanoparticle-containing simulations with those obtained in the corresponding nanoparticle-free reference medium [19,20].

2.10 Statistical Uncertainty

The number of primary particle histories was selected individually for each simulation to maintain statistical uncertainties below approximately 5% within the principal scoring regions. Larger statistical uncertainties were observed at increasing distances from the nanoparticle surface because of the lower interaction probability and reduced particle fluence. Unless otherwise stated, all reported uncertainties correspond to one standard deviation (1σ) of the Monte Carlo statistical error.

3. Results

3.1 Dose Enhancement Factor

All investigated nanoparticles increased local dose deposition compared with the corresponding nanoparticle-free reference media. The magnitude of dose enhancement strongly depended on nanoparticle composition, atomic number, and the surrounding medium.

As shown in Figure 5, the dose enhancement factor (DEF) varied considerably among the evaluated nanoparticle materials. Tantalum (Ta) nanoparticles exhibited the highest DEF values, followed by platinum (Pt) and gold (Au) nanoparticles, whereas lower-atomic-number materials, including iron (Fe) and titanium (Ti), produced substantially weaker enhancement effects.

The maximum dose enhancement occurred at the shortest radial distances adjacent to the nanoparticle surface, where secondary electron generation and local energy deposition were most pronounced. For gold nanoparticles, the absorbed dose increased by approximately 12-fold compared with the nanoparticle-free reference medium (DEF ≈ 13). The enhancement gradually decreased with increasing distance from the nanoparticle surface due to electron transport and energy dissipation, although measurable enhancement persisted over micrometer-scale distances.

The surrounding medium also affected energy deposition patterns. Simulations performed in PEG polymer demonstrated higher absolute absorbed doses compared with those conducted in water, likely due to differences in material density and elemental composition. However, after normalization to the corresponding nanoparticle-free

reference medium, DEF values were generally lower in PEG than in water. This indicates that although PEG increased overall energy deposition, it reduced the relative contribution of nanoparticles to dose amplification.

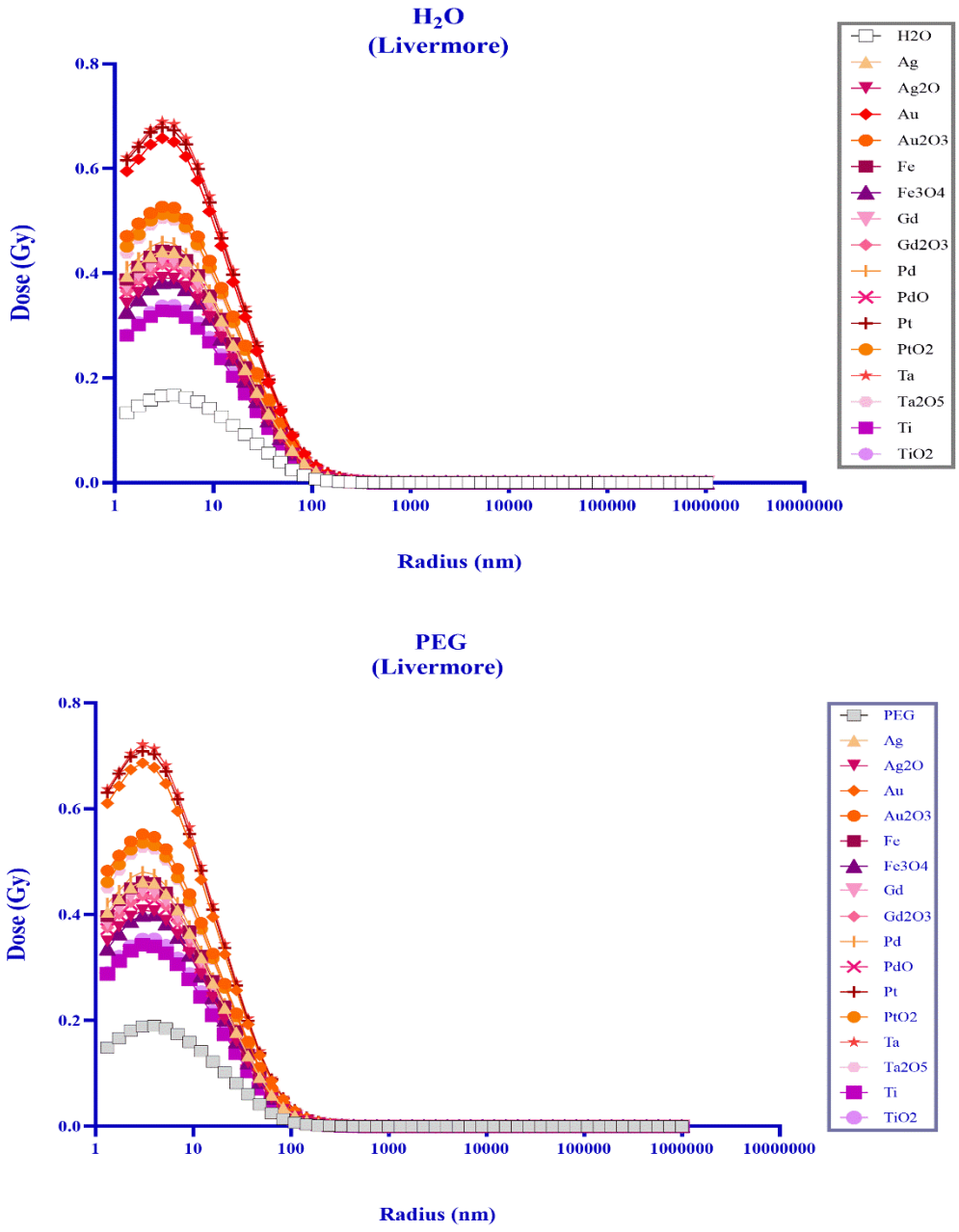


Figure 5. Comparison of dose enhancement factors (DEFs) for the investigated nanoparticles in water and PEG polymer media.

3.2 Effect of Nanoparticle Oxidation State on Dose Enhancement

The influence of nanoparticle oxidation state on dose enhancement was investigated by comparing elemental metallic nanoparticles with their corresponding oxide forms in both water and PEG polymer media. Across all investigated materials, elemental metals consistently produced higher dose enhancement factors (DEFs) than their oxide counterparts, irrespective of the electromagnetic physics model employed. This trend was particularly evident for high-Z nanoparticles, with tantalum (Ta), platinum (Pt), and gold (Au) exhibiting the highest DEF values, whereas iron (Fe) and titanium (Ti) nanoparticles showed substantially lower enhancement.

Oxide nanoparticles consistently generated lower DEF values than the corresponding elemental metals throughout the investigated radial distances. The enhancement trend remained unchanged in both media, following the order:

Ta > Pt > Au > corresponding metal oxides > Fe- and Ti-based nanoparticles.

The reduction in DEF observed for oxide nanoparticles was consistent throughout the simulation domain and exceeded the statistical uncertainties of the calculations, indicating that the differences reflected material-dependent characteristics rather than simulation variability.

Comparison of the Livermore and Penelope electromagnetic physics models revealed highly consistent material-dependent trends. Although minor quantitative differences were observed between the two transport models, both predicted the same nanoparticle ranking, demonstrating that nanoparticle composition and oxidation state exerted a greater influence on dose enhancement than the choice of electromagnetic physics model.

As shown in Figure 6, the superiority of elemental metallic nanoparticles over their oxide counterparts was preserved in PEG polymer, confirming the same material-dependent behavior observed in water. Figure 7 further compares the absorbed dose distributions in water and PEG media using both electromagnetic physics models. PEG exhibited higher absolute energy deposition than water because of its higher density and interaction probability. However, nanoparticle-induced dose enhancement should be interpreted using DEF values normalized to the corresponding nanoparticle-free reference medium rather than absolute absorbed dose alone.

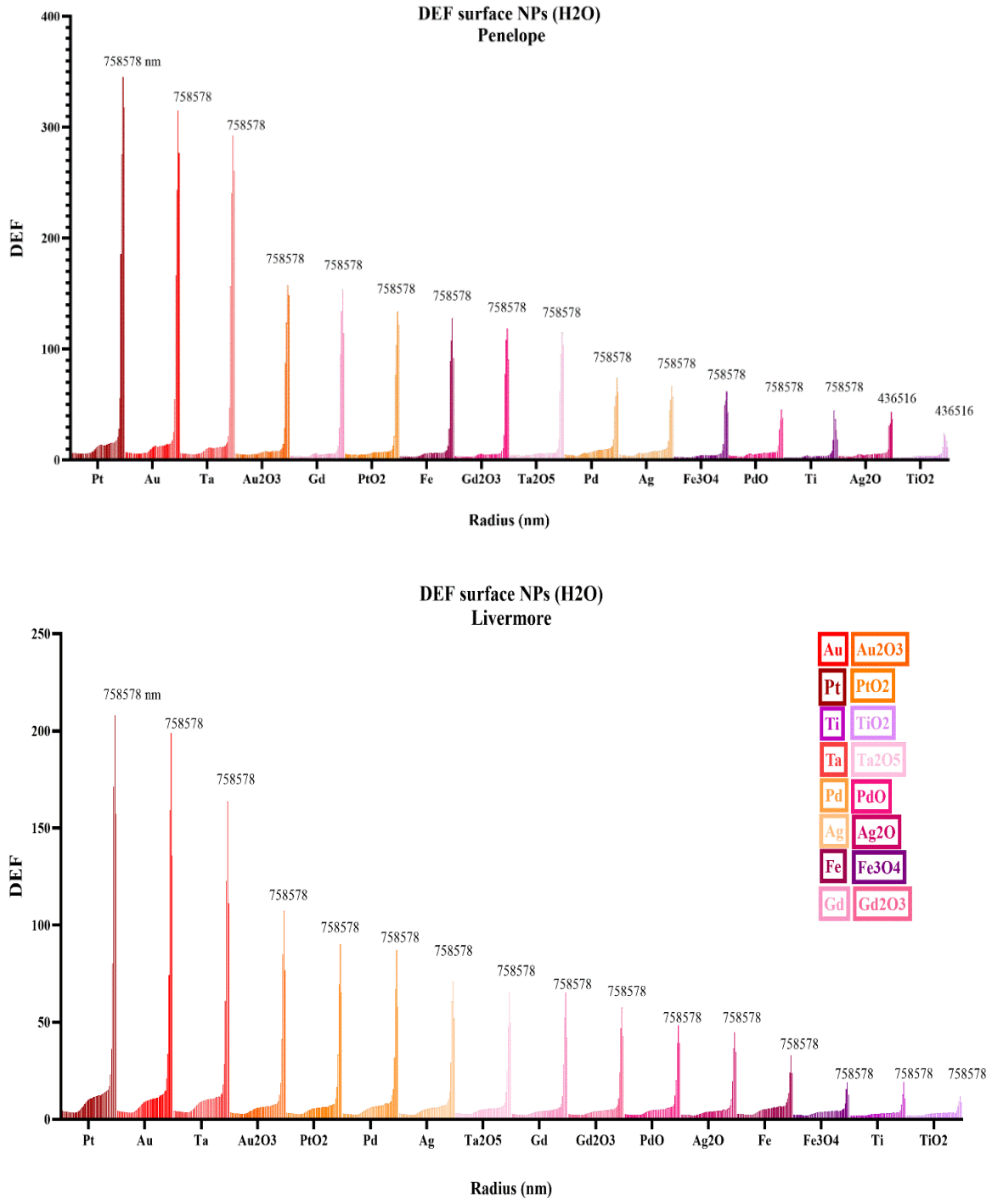


Figure 6. Comparison of dose enhancement factors for metallic nanoparticles and their oxide forms in water using Livermore and Penelope electromagnetic physics models.

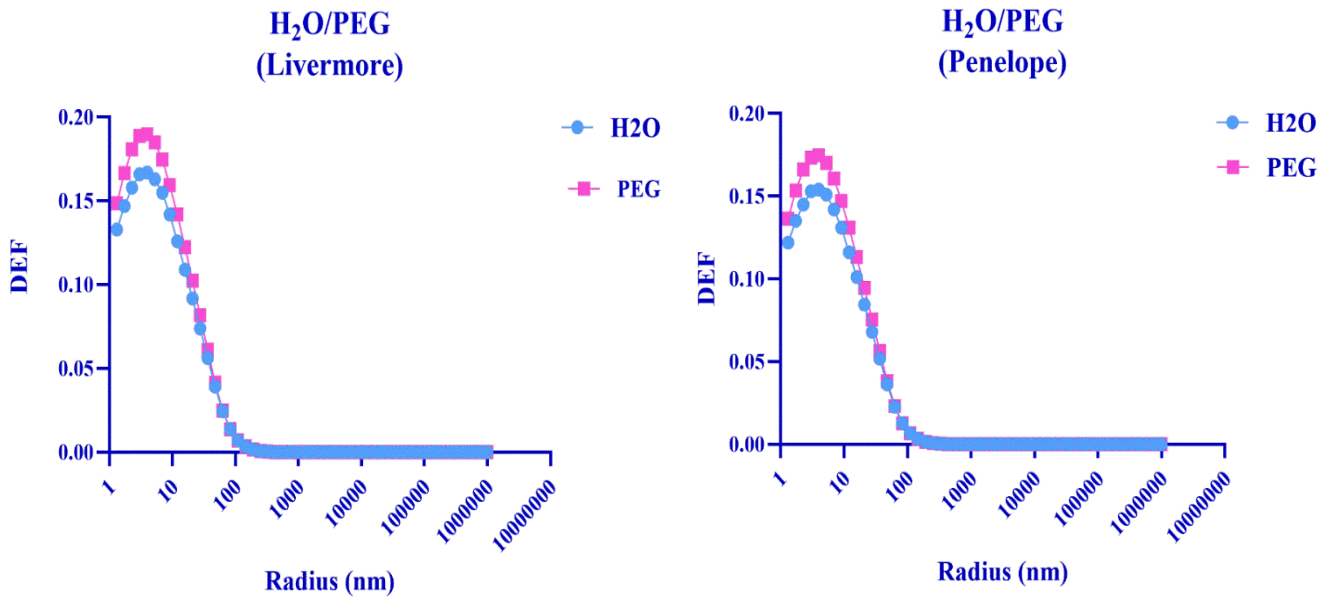


Figure 7. Comparison of absorbed dose deposition in water and PEG polymer media using Livermore and Penelope electromagnetic physics models.

3.3 Secondary Particle Production

Secondary particle production was strongly dependent on nanoparticle composition and atomic number. Overall, high-Z nanoparticles generated substantially greater numbers of secondary electrons than lower-Z materials, reflecting their enhanced interaction probability with the emitted β particles.

Among the investigated materials, platinum nanoparticles produced the highest secondary electron yield, followed by gold and tantalum nanoparticles. In contrast, iron- and titanium-based nanoparticles generated considerably fewer secondary electrons under identical irradiation conditions. The enhanced production of secondary electrons by high-Z nanoparticles is consistent with the increased local energy deposition observed in the DEF analysis. These material-dependent differences in secondary electron yields are illustrated in Figure 8.

Comparison of the Livermore and Penelope electromagnetic physics models demonstrated similar material-dependent trends. Although the Penelope model predicted slightly higher secondary electron yields than the Livermore model, the relative ranking of nanoparticle materials remained unchanged, indicating that the observed differences were primarily associated with nanoparticle composition rather than the selected transport model.

The surrounding medium also influenced secondary particle production. Simulations performed in PEG polymer yielded approximately 5–10% higher absolute secondary electron production than those performed in water, consistent with the higher density of the polymeric medium. No positron production was detected in any simulation because β^- decay of ^{177}Lu does not generate positrons.

Complete quantitative results for secondary particle production under all simulation conditions are provided in the Supplementary Information.

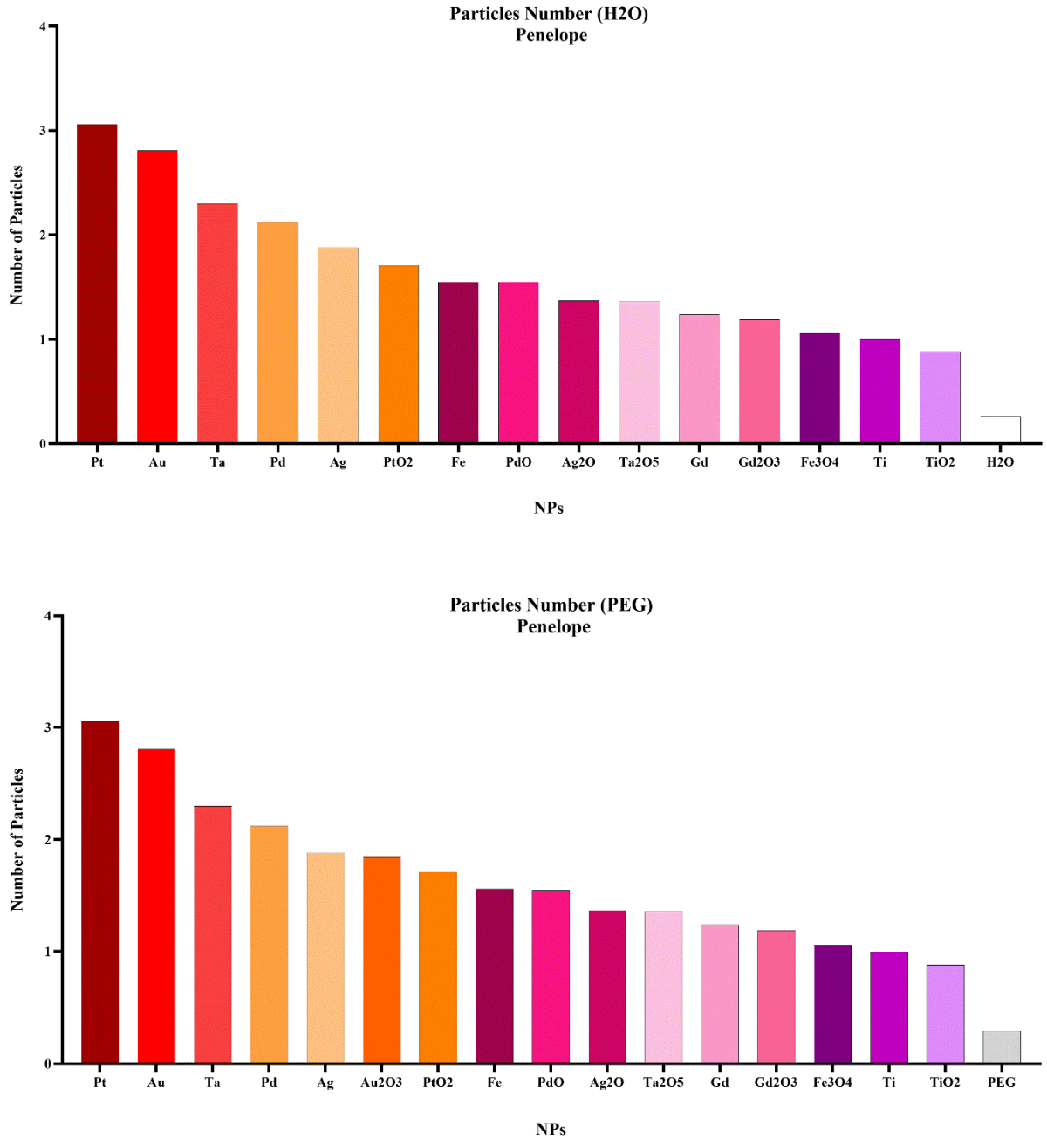


Figure 8. Secondary electron yields of the investigated metallic nanoparticles and their corresponding oxides in water and PEG polymer media predicted using the Penelope electromagnetic physics model.

3.4 Physical Interaction Processes

The principal electromagnetic interaction processes were analyzed for all investigated nanoparticle materials in both water and PEG polymer media. Ionization was the predominant interaction mechanism under all simulation conditions and represented the largest contribution to local energy deposition.

High-Z nanoparticles exhibited substantially greater interaction yields than lower-Z materials, particularly for ionization, Auger electron emission, and characteristic X-ray production. Platinum, gold, and tantalum nanoparticles generated the highest yields of characteristic secondary emissions, whereas iron- and titanium-based nanoparticles consistently exhibited lower interaction frequencies. These findings are consistent with the enhanced dose deposition observed for high-Z materials in the DEF analysis.

Comparison of the Livermore and Penelope electromagnetic physics models demonstrated highly similar interaction patterns. Although minor quantitative differences were observed between the two models, both predicted the same material-dependent trends, indicating that nanoparticle composition exerted a greater influence on interaction yields than the selected electromagnetic transport model.

The surrounding medium also influenced the frequency of physical interactions. Simulations performed in PEG polymer generally produced higher interaction yields than those performed in water because of the higher density of the polymeric medium. However, the relative ranking of the investigated nanoparticle materials remained unchanged across both media.

Figure 9 compares the number of physical interaction events for the investigated metallic nanoparticles and their corresponding oxides in water and PEG polymer media using the Livermore electromagnetic physics model. Ionization was the dominant interaction process for all investigated materials, whereas high-Z nanoparticles consistently generated higher numbers of Auger electrons and characteristic X-rays than lower-Z materials. Complete quantitative results for all physical interaction processes are provided in the Supplementary Information.

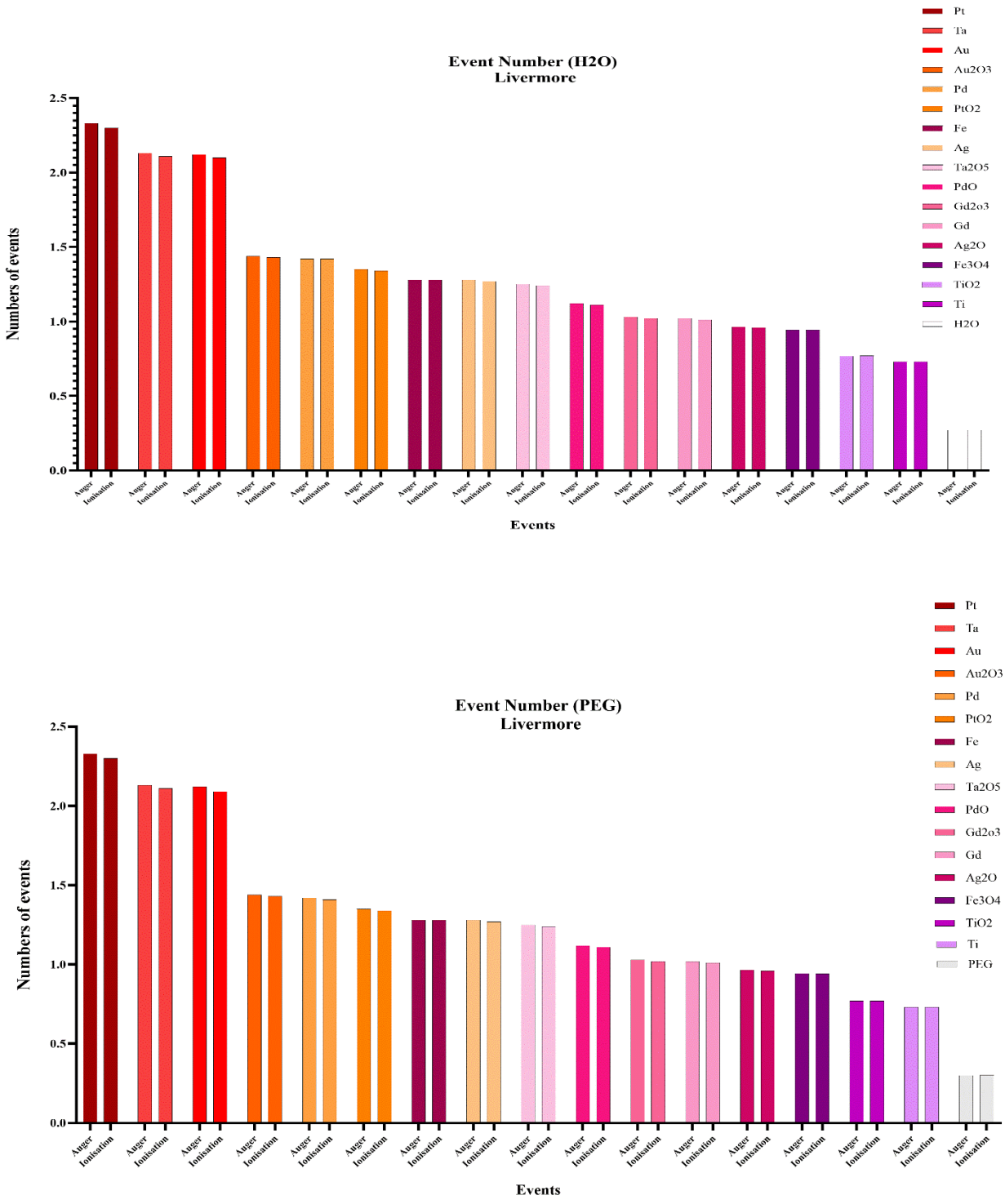


Figure 9. Comparison of physical interaction events for the investigated metallic nanoparticles and their corresponding oxides in water and PEG polymer media using the Livermore electromagnetic physics model.

3.5 DNA Damage

The incorporation of high-Z nanoparticles increased both direct and indirect DNA damage compared with the corresponding nanoparticle-free reference media. The enhancement was observed for all investigated damage endpoints, including single-strand breaks (SSBs), double-strand breaks (DSBs), and hybrid DSBs.

Among the investigated materials, gold nanoparticles produced the highest frequencies of DNA damage, followed by platinum and tantalum nanoparticles. This behavior is consistent with their enhanced secondary electron production and increased local energy deposition at the nanoscale. In contrast, iron- and titanium-based nanoparticles generated considerably lower levels of DNA damage.

Indirect DNA damage mediated by hydroxyl radicals (•OH) represented the predominant contribution to the overall DNA damage, exceeding the frequency of direct strand breaks under all simulation conditions. This observation highlights the important role of radiation-induced chemical species in nanoparticle-enhanced β-particle therapy.

The surrounding medium also influenced DNA damage induction. Simulations performed in PEG polymer produced higher absolute frequencies of SSBs, DSBs, and hybrid DSBs than those performed in water, reflecting the greater interaction probability associated with the higher density of the polymeric medium. Nevertheless, the relative ranking of nanoparticle materials remained unchanged across both media.

The Livermore and Penelope electromagnetic physics models predicted highly consistent DNA damage patterns. Although the Penelope model generally yielded slightly higher damage frequencies, both physics models produced the same material-dependent trends.

Figures 10 and 11 compare the simulated DNA damage yields for the investigated metallic nanoparticles and their corresponding oxides using the Livermore and Penelope electromagnetic physics models. In both water and PEG polymer media, high-Z nanoparticles produced greater DNA damage than low-Z materials, while gold nanoparticles exhibited the highest frequencies of SSBs, DSBs, and hybrid DSBs. Although absolute DNA damage yields were higher in PEG polymer than in water, the relative ranking of the investigated nanoparticle materials remained unchanged across both media.

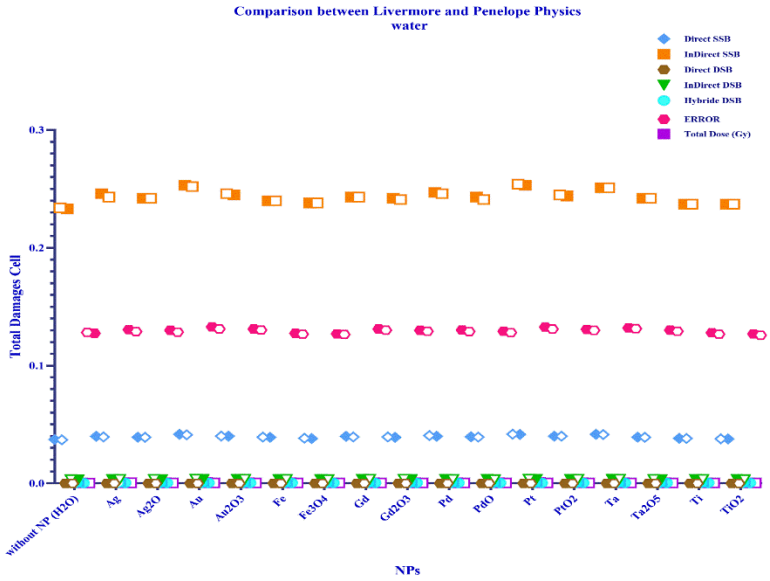


Figure 10. Comparison of simulated DNA damage yields induced by the investigated metallic nanoparticles and their corresponding oxide forms in water medium using the Livermore and Penelope electromagnetic physics models.

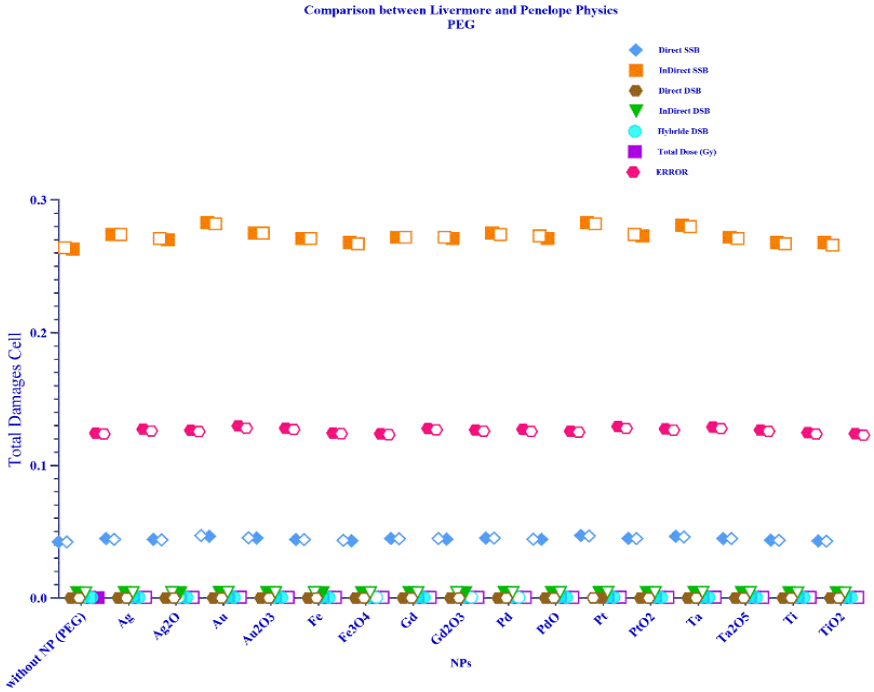


Figure 11. Comparison of simulated DNA damage yields induced by the investigated metallic nanoparticles and their corresponding oxide forms in PEG polymer medium using the Livermore and Penelope electromagnetic physics models.

3.6 Chemical Species Production

The production of radiation-induced chemical species was enhanced in the presence of nanoparticles, with a more pronounced increase observed for high-Z materials. In the aqueous medium, hydroxyl radicals (•OH) and hydrated electrons (e^-_{aq}) were the dominant species, followed by hydrogen peroxide (H_2O_2) and hydrogen radicals (H•). The enhanced production of reactive species in nanoparticle-containing systems can be attributed to increased local energy deposition and secondary electron generation around the nanoparticle surface.

In PEG polymer medium, the absolute yields of chemical species were higher than those observed in water, which is related to the differences in medium density and energy deposition characteristics. However, the relative response pattern among different nanoparticle compositions remained consistent across both media and electromagnetic physics models, with high-Z nanoparticles exhibiting stronger chemical enhancement compared with lower-Z materials.

The simulations considered the contribution of various radiolytic species, including H_2O_2, H_2O, H_3O^+, HO_2•, H•, H_2, •OH, OH^-, O_2^-, O_2, O_3, and e^-_{aq}. The complete quantitative data for all generated chemical species under different nanoparticle conditions, media, and physics models are provided in the Supplementary Information. Figures 10 and 11 summarize the yields of the major biologically relevant chemical species in water and PEG media, respectively. Among the investigated species, •OH and e^-_{aq} showed the highest production levels for both Livermore and Penelope electromagnetic physics models. Nanoparticle incorporation increased the generation of these reactive species, particularly for high-Z nanoparticles. Since highly reactive species such as •OH have a limited diffusion range, typically within a few nanometers from their generation site, their increased local production may contribute to the enhanced DNA damage observed in nanoparticle-containing systems.

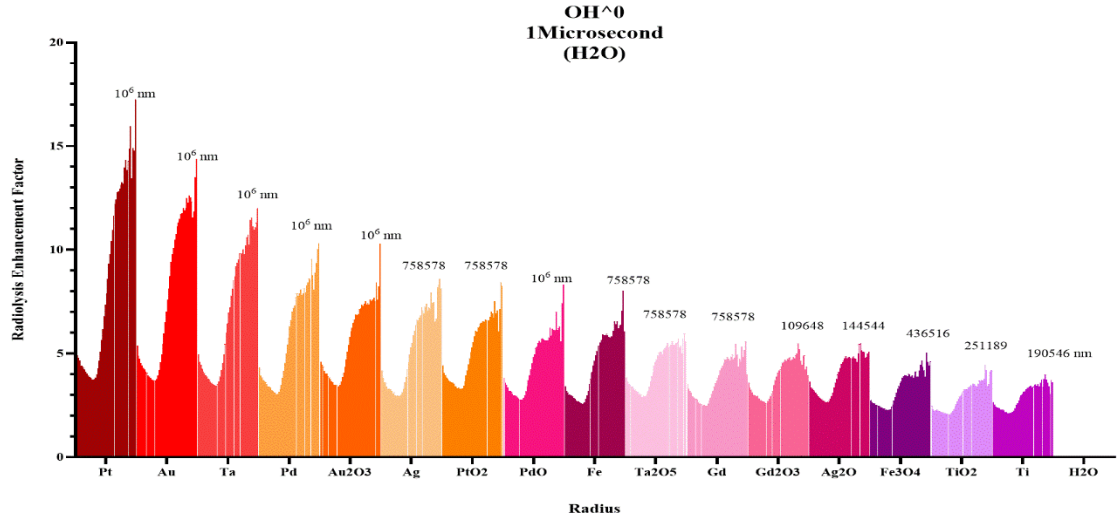
3.7 Radical Enhancement Factor (REF)

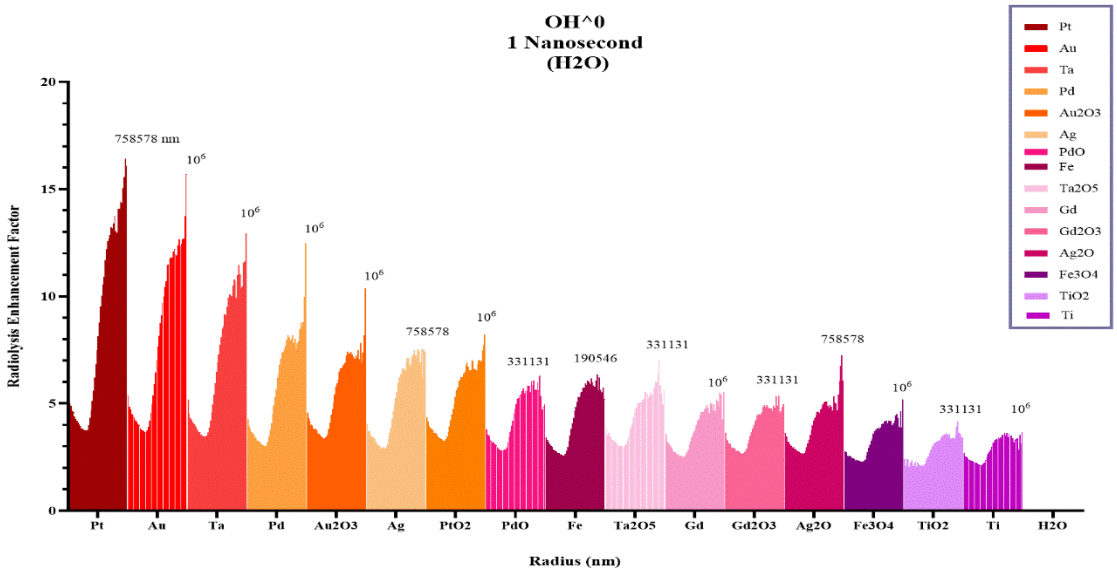
REF values were highest at the earliest chemical stage (10 ps) and progressively decreased with increasing chemical-stage time and radial distance from the nanoparticle surface. This reduction is attributed to the diffusion, recombination, and chemical reactions of reactive species, which decrease the number of free radicals available within the surrounding medium over time.

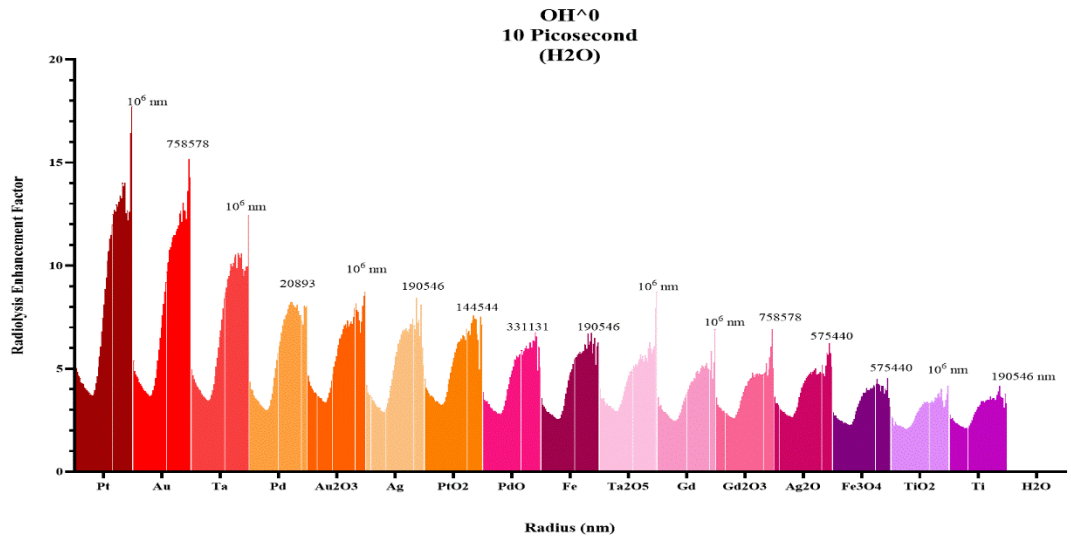
At 1 ns, REF values decreased by approximately 30–50% compared with the initial stage, while at 1 μs, most reactive species had undergone diffusion, recombination, or chemical transformation, resulting in REF values approaching unity except at very short distances near the nanoparticle surface. The strongest enhancement was observed within the first tens of nanometers, where the concentration of radiation-induced species remained higher due to localized energy deposition and limited diffusion.

The spatial distribution of REF was influenced by the detection volume, with smaller regions near the nanoparticle surface showing greater sensitivity to short-range radical enhancement. Since highly reactive species such as hydroxyl radicals (•OH) have limited diffusion ranges, typically within a few nanometers, their contribution is primarily observed in the immediate vicinity of the nanoparticle surface.

Figure 12 illustrates the REF kinetics of hydroxyl radical (•OH) production in water and PEG polymer media using the Livermore electromagnetic physics model in the presence of nanoparticles. The results indicate that nanoparticle-induced enhancement of reactive species production is transient and strongly dependent on both chemical-stage time and distance from the nanoparticle surface.


OH^0
1Microsecond
(H2O)
Radiolysis Enhancement Factor
Radius
Pt
Au
Ta
Pd
Au2O3
Ag
PtO2
PdO
Fe
Ta2O5
Gd
Gd2O3
Ag2O
Fe3O4
TiO2
Ti
H2O
10^6 nm
758578
109648
144544
436516
251189
190546 nm


OH^0
1 Nanosecond
(H2O)
Radiolysis Enhancement Factor
Radius (nm)
Pt
Au
Ta
Pd
Au2O3
Ag
PtO2
PdO
Fe
Ta2O5
Gd
Gd2O3
Ag2O
Fe3O4
TiO2
Ti
H2O
758578 nm
10^6
758578
331131
190546
331131
758578


OH^0
10 Picosecond
(H2O)
Radiolysis Enhancement Factor
Radius (nm)
Pt
Au
Ta
Pd
Au2O3
Ag
PtO2
PdO
Fe
Ta2O5
Gd
Gd2O3
Ag2O
Fe3O4
TiO2
Ti
H2O
10^6 nm
758578
20893
190546
144544
331131
575440
190546 nm

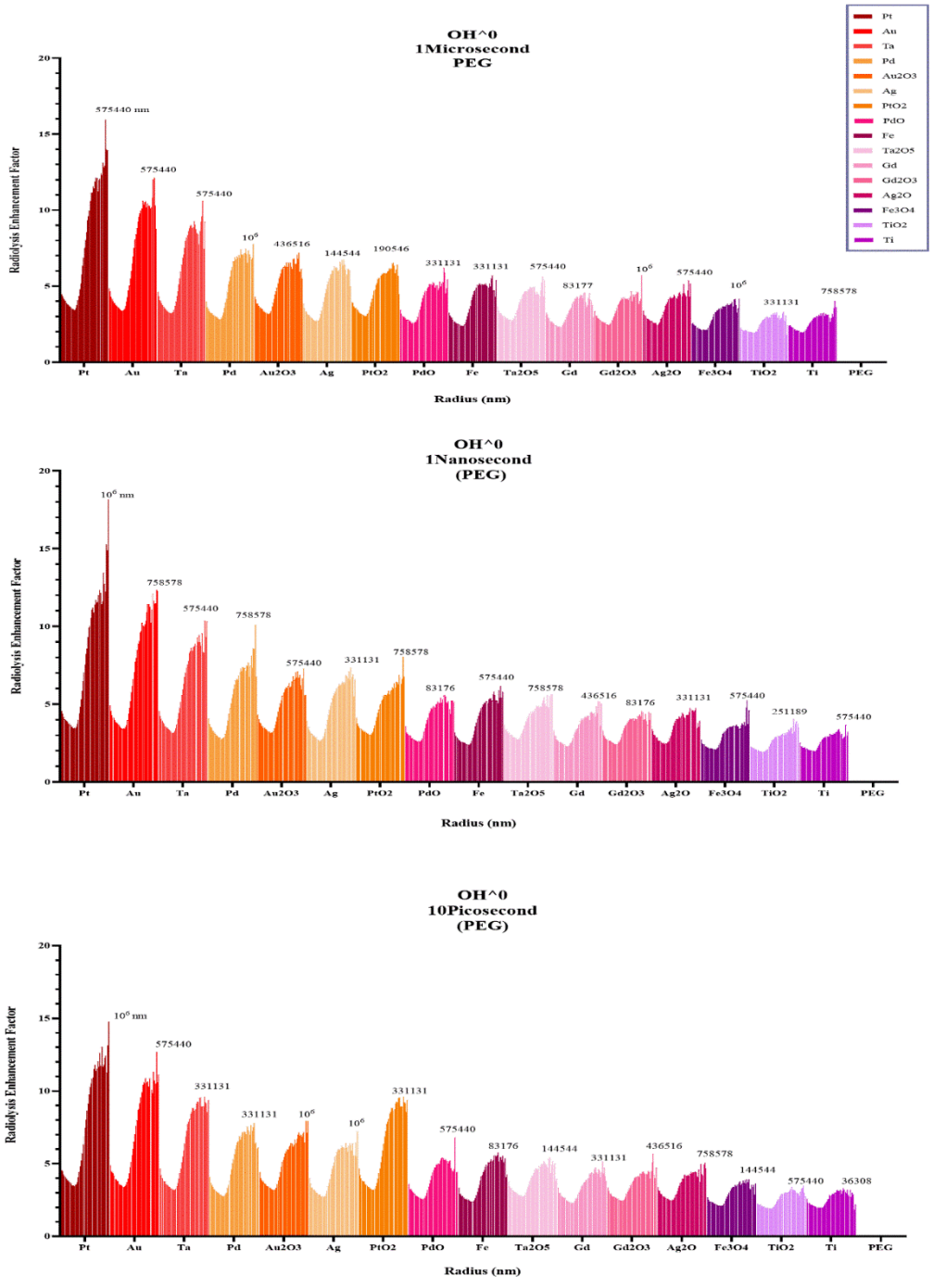


Figure 12. REF kinetics of hydroxyl radical (•OH) production for the investigated metallic nanoparticles and their corresponding oxide forms in water and PEG polymer media at 10 ps, 1 ns, and 1 µs chemical-stage times.

4. Discussion

The present study provides a comprehensive multiscale evaluation of nanoparticle-assisted 177Lu targeted radionuclide therapy by integrating physical dose deposition, secondary particle production, radiation chemistry, and DNA damage within a unified Geant4-DNA simulation framework. Unlike many previous Monte Carlo investigations that have primarily focused on gold nanoparticles under external photon irradiation, this work systematically compared multiple high-Z metallic nanoparticles and their corresponding oxides under beta-particle irradiation in both aqueous and PEG-based environments. The results demonstrate that nanoparticle composition, oxidation state, surrounding medium, and the selected electromagnetic physics model collectively influence radiation enhancement, although their contributions differ depending on the investigated endpoint.

Overall, high-Z nanoparticles substantially enhanced radiation-induced physical, chemical, and biological effects compared with nanoparticle-free media. However, the relative ranking of nanoparticle performance depended on the evaluated parameter. Tantalum exhibited the greatest dose enhancement, platinum generated the highest secondary electron yields, and gold produced the largest increase in simulated DNA damage. These findings indicate that nanoparticle radiosensitization cannot be adequately described using a single performance metric and instead reflects the combined influence of multiple physical and biological mechanisms. [21-24]

4.1 Dose Enhancement Induced by High-Z Nanoparticles

The observed increase in dose enhancement near the nanoparticle surface is consistent with the fundamental interaction mechanisms governing beta-particle transport in high-Z materials. As energetic electrons emitted by 177Lu penetrate metallic nanoparticles, multiple inelastic collisions generate cascades of low-energy secondary electrons that deposit their energy over nanometer-scale distances surrounding the nanoparticle. Consequently, energy deposition becomes highly localized despite the relatively long range of the primary beta particles.

Among the investigated materials, tantalum consistently produced the highest dose enhancement factors in both water and PEG media. [25,26] This behavior is primarily attributed to its favorable combination of high atomic number, material density, and electron stopping characteristics, which collectively increase local interaction probability and energy deposition. Platinum and gold also exhibited pronounced dose amplification, although their enhancement

remained slightly lower than that of tantalum throughout most radial distances. In contrast, iron and titanium generated considerably smaller dose enhancement because their lower atomic numbers reduce the probability of secondary electron production.

An important observation was the rapid decrease in DEF with increasing distance from the nanoparticle surface. This spatial behavior reflects the limited penetration range of low-energy secondary electrons generated within the nanoparticle. Most of the additional energy deposition therefore remains confined to the immediate nanoparticle microenvironment, emphasizing that nanoparticle radiosensitization is fundamentally a nanoscale phenomenon. This highly localized energy amplification may be particularly advantageous for targeted radionuclide therapy because it increases intracellular radiation damage while minimizing unnecessary dose deposition in surrounding healthy tissues.[27]

The comparison between water and PEG media further demonstrated that although PEG exhibited higher absolute absorbed doses owing to its greater density, normalization against the corresponding nanoparticle-free reference medium resulted in lower relative DEF values than those observed in water. This distinction highlights the importance of separating absolute energy deposition from true nanoparticle-induced dose enhancement when comparing different biological environments.

4.2 Influence of Nanoparticle Oxidation State

The comparison between elemental metals and their corresponding oxides demonstrated that oxidation consistently reduced dose enhancement across all investigated materials. This reduction is expected because oxide formation decreases the effective atomic number and modifies the electronic structure of the nanoparticle, thereby reducing the efficiency of secondary electron generation following beta-particle interactions.

Although oxide nanoparticles retained measurable radiosensitizing capability, their performance remained consistently inferior to that of their corresponding pure metallic forms. The same material-dependent trend was preserved in both water and PEG media and was reproduced by both electromagnetic physics models, indicating that oxidation state represents an intrinsic material property rather than a model-dependent computational artifact.

These findings have practical implications for nanoparticle synthesis and surface engineering. While oxide nanoparticles often exhibit improved chemical stability and biocompatibility, their reduced radiation enhancement should be considered during the design of nanoparticle-based radionuclide therapies. Future optimization strategies should therefore balance physicochemical stability with radiation amplification efficiency.

4.3 Secondary Electron Production and Physical Interaction Mechanisms

Secondary electron production represents one of the principal mechanisms underlying nanoparticle-mediated radiosensitization. Unlike external photon irradiation, where photoelectric interactions dominate energy amplification, beta-particle irradiation primarily enhances radiation effects through successive ionization events and the generation of low-energy secondary electrons. These electrons possess short penetration ranges and high linear energy transfer (LET) over nanometer-scale distances, enabling highly localized energy deposition in the vicinity of the nanoparticle.

Although tantalum exhibited the highest dose enhancement, platinum generated the largest number of secondary electrons in the present simulations. This observation indicates that overall dose enhancement is not determined solely by the total number of emitted secondary electrons but also by their energy distribution, transport characteristics, and deposition efficiency within the surrounding medium. Consequently, different nanoparticle materials may exhibit distinct rankings depending on whether the evaluated endpoint is absorbed dose, secondary electron production, or biological damage.

The dominance of ionization observed in all investigated materials is consistent with the interaction mechanisms expected for medium-energy beta particles emitted by 177Lu. In contrast, Auger electron production and characteristic X-ray emission increased markedly with increasing atomic number. Platinum and gold generated the highest Auger electron yields, reflecting the greater probability of inner-shell ionization in high-Z materials. Although Auger electrons contribute only minimally to macroscopic absorbed dose, their extremely short range allows highly concentrated energy deposition at nanometer dimensions, thereby increasing the probability of localized biological damage.

The comparison between the Livermore and Penelope electromagnetic physics models demonstrated highly consistent trends in material-dependent radiation enhancement. Penelope generally predicted slightly higher secondary electron

yields than Livermore, which is likely related to differences in low-energy electron transport algorithms and interaction cross-sections implemented in the two physics models. Nevertheless, the overall agreement between both models supports the robustness of the observed enhancement patterns and indicates that the primary conclusions are largely independent of the selected electromagnetic physics configuration.

4.4 Radiation Chemistry and DNA Damage

The physical amplification of energy deposition observed in the presence of high-Z nanoparticles was accompanied by a corresponding increase in radiation-induced chemical species and DNA damage. This finding reflects the sequential relationship between the physical, physicochemical, and chemical stages of radiation action. Increased secondary electron production during the physical stage generates a greater number of ionization and excitation events within the surrounding medium, ultimately leading to enhanced water radiolysis and increased formation of reactive oxygen species during the chemical stage.

Hydroxyl radicals (•OH) represented the dominant chemically mediated species contributing to indirect DNA damage, consistent with the established role of hydroxyl radicals in radiation biology. Because these radicals exhibit extremely high chemical reactivity but limited diffusion distances, the localized increase in radical concentration surrounding high-Z nanoparticles contributes substantially to nanoscale biological amplification. The calculated REF values further demonstrated that radical concentrations were greatest immediately after irradiation and progressively decreased with increasing chemical-stage time owing to diffusion, recombination, and chemical reactions. By approximately 1 μs, most reactive species had either recombined or reacted, causing REF values to approach unity except within the immediate vicinity of the nanoparticle surface. [28,29]

Although platinum generated the largest number of secondary electrons, gold produced the highest frequency of simulated DNA damage. This apparent discrepancy emphasizes that DNA damage depends not only on the quantity of secondary electrons but also on their spatial distribution, energy spectrum, and ability to generate reactive chemical species in biologically relevant locations. Therefore, physical dose enhancement alone cannot fully predict biological effectiveness, highlighting the importance of integrating physical, chemical, and biological simulations within a single computational framework.[30]

The influence of the surrounding medium was also evident during the chemical stage. PEG-based simulations produced higher absolute radical yields and DNA damage than water because of increased energy deposition within the denser medium. However, the relative enhancement pattern among nanoparticle materials remained largely unchanged, suggesting that nanoparticle composition exerts a stronger influence on radiosensitization than the surrounding medium itself. These findings indicate that although biological media modify the magnitude of radiation interactions, they do not substantially alter the comparative performance of different nanoparticle materials.

4.5 Clinical and Translational Relevance

The present findings have important implications for the future development of nanoparticle-assisted targeted radionuclide therapy (TRT). Unlike external beam radiotherapy, radionuclide therapy delivers radiation continuously over extended periods and at relatively low dose rates. Consequently, strategies capable of locally amplifying radiation effects without increasing administered radioactivity are of considerable clinical interest. The present simulations indicate that appropriately selected high-Z nanoparticles can substantially enhance local energy deposition, secondary electron production, radiation chemistry, and DNA damage while preserving the favorable dosimetric characteristics of 177Lu.

Among the investigated materials, tantalum exhibited the greatest dose enhancement capability, whereas platinum generated the highest secondary electron yields and gold produced the highest simulated DNA damage. These findings suggest that the optimal nanoparticle material may depend on the intended therapeutic endpoint. Therefore, nanoparticle selection should not rely solely on physical dose enhancement but should also consider downstream biological effects and the desired therapeutic mechanism.

The influence of the surrounding medium further emphasizes the importance of incorporating biologically relevant environments into computational investigations. Although PEG-based simulations resulted in higher absolute energy deposition than water, the relative enhancement ranking of the investigated nanoparticles remained largely unchanged. This observation suggests that the radiosensitizing potential of high-Z nanoparticles is primarily governed by intrinsic material properties rather than by moderate variations in the surrounding medium.

From a translational perspective, these results may contribute to the rational design of nanoparticle-based radiosensitizers for targeted radionuclide therapy. Computational optimization of nanoparticle composition before experimental evaluation may reduce development costs, improve candidate selection, and facilitate the design of more effective nanomedicine platforms for radionuclide delivery.

4.6 Study Limitations and Future Perspectives

Several limitations should be considered when interpreting the present findings.

First, all simulations were performed using nanoparticles with a fixed radius of 25 nm. Because nanoparticle size strongly influences electron emission, energy deposition, cellular internalization, and biodistribution, future investigations should evaluate a wider range of particle sizes and geometries.

Second, the present study focused on isolated nanoparticles and simplified intracellular distributions. In biological systems, nanoparticle aggregation, heterogeneous intracellular localization, and variable intracellular concentrations may alter both physical interactions and biological responses. Incorporating these factors into future simulations would improve physiological realism.

Third, DNA damage calculations were limited to the initial induction of strand breaks and did not include subsequent biological processes such as DNA repair, cell-cycle redistribution, apoptosis, or long-term cellular responses. Consequently, the simulated DNA damage should be interpreted as an indicator of initial biological effectiveness rather than a direct prediction of therapeutic outcome.

In addition, the surrounding media were represented by water and PEG polymer as simplified models of biological environments. Although PEG provides a more realistic approximation than pure water for nanoparticle-coated systems, actual intracellular conditions involve substantially greater chemical complexity, including proteins, lipids, organelles, and heterogeneous molecular compositions that may further influence radiation chemistry and radical transport.

Finally, the present work is based entirely on Monte Carlo simulations and has not yet been validated experimentally. Future studies combining computational modeling with in vitro and in vivo investigations will be necessary to confirm

the predicted dose enhancement, radical production, and DNA damage induced by high-Z nanoparticles during 177Lu irradiation.

Despite these limitations, the present study provides a comprehensive multiscale computational framework integrating physical interactions, radiation chemistry, and biological damage within a unified Geant4-DNA simulation environment. Such an integrated approach offers valuable mechanistic insight into nanoparticle-enhanced targeted radionuclide therapy and provides a foundation for future computational and experimental optimization.

5. Conclusion

This study systematically investigated the physical, chemical, and biological effects of high-Z nanoparticles during 177Lu-targeted radionuclide therapy using a multiscale Geant4-DNA Monte Carlo simulation framework. By integrating nanoparticle-scale dose calculations with cellular DNA damage and radiolysis simulations, the study provides a comprehensive evaluation of nanoparticle-mediated radiosensitization under biologically relevant conditions.

The results demonstrated that high-Z nanoparticles significantly enhanced local energy deposition, secondary particle production, reactive chemical species generation, and radiation-induced DNA damage compared with nanoparticle-free conditions. The magnitude of these effects depended strongly on nanoparticle composition, oxidation state, and the surrounding medium. Pure metallic nanoparticles consistently produced greater dose enhancement than their corresponding oxides, while PEG-based media resulted in higher absolute energy deposition than water because of their increased density. Although the two electromagnetic physics models (Livermore and Penelope) produced slight quantitative differences, both generated highly consistent material-dependent enhancement trends, supporting the robustness of the simulation results.

Importantly, the present study demonstrates that different biological and physical endpoints do not necessarily exhibit identical material rankings. Tantalum nanoparticles produced the highest dose enhancement, platinum generated the greatest secondary electron yields, and gold induced the highest levels of simulated DNA damage. These findings indicate that nanoparticle selection for targeted radionuclide therapy should be guided by the intended therapeutic objective rather than by a single dosimetric parameter. Overall, this work provides mechanistic insight into the multiscale processes underlying nanoparticle-enhanced 177Lu therapy and establishes a computational framework for

evaluating candidate radiosensitizers before experimental investigation. The findings support the continued development of high-Z nanoparticle platforms and may contribute to the rational design and optimization of next-generation nanoparticle-assisted targeted radionuclide therapies.

Declarations

Funding: This study was supported by the Deputy of Research, Tehran University of Medical Sciences (TUMS), Tehran, Iran (Grant No. 1400-3-101-55359). The funding body had no role in the design of the study; collection, analysis, or interpretation of the data; or writing of the manuscript.

Competing interests: The authors declare that they have no competing interests.

Ethics approval and consent to participate: Not applicable.

Consent to publish: Not applicable.

Data availability: All data generated or analyzed during this study are included in this published article and its supplementary information files.

Acknowledgements: Not applicable.

Author Contributions: Fatemeh Mahdavi: Conceptualization, Methodology, Software, Writing – original draft. Developed the adaptive importance sampling estimator and implemented the simulation code. Amir Reza Jalilian: Investigation, Data curation. Ran benchmark experiments and curated simulation datasets. Fariba Esmaili: Writing-review & editing. Contributed to manuscript writing, editing, and revision. Parham Geramifar and Sharmin Kharrazi: Supervision and oversaw the project, Funding acquisition, Project administration, Writing – review & editing.

References:

1.Xiaohan Ma, et al Nanotechnology in healthcare, and its safety and environmental risks, Journal of Nanobiotechnology ,22:715, 2024.

2.Laure Vergnaud, Yuni K Dewaraja, Anne-Laure Giraudet, Jean-Noël Badel, David Sarrut. A review of 177Lu dosimetry workflows: how to reduce the imaging workloads? EJNMMI Phys, 2024 Jul 18;11(1):65.

3.Jing Jin & Qijie Zhao, Engineering nanoparticles to reprogram radiotherapy and immunotherapy: recent advances and future challenges, Journal of Nanobiotechnology, 18, 75 (2020).

4.Yi Zhu, Guobiao Zhong, Wei Zhang, Weijun Wei, Binxu Yin & Kun Zhang Combination therapy strategies in engineered 177Lu radiopharmaceuticals beyond single modality: design principles and application outlet, Cell Communication and Signaling, 2026, 24, 133.

5.Sakata, D., Kyriakou, I., Okada, S., et al. *Geant4-DNA track-structure simulations for gold nanoparticles: The importance of electron discrete models in nanometer volumes. * Medical Physics, 2018, 45(5), 2230–2242.

6.Taylan Tuğrul, Dose enhancement effects of different-sized nanoparticles on tumors and surrounding tissues using Geant4 track structure simulation, J Nukleonika. (September 2025) Volume 70

7.Chloe Doen Kim and James C. L. Chow, Reactive Oxygen Species Yield near Gold Nanoparticles Under Ultrahigh-Dose-Rate Electron Beams: A Monte Carlo Study. Nanomaterials, 2025,15(17), 1303.

8.Hoang Ngoc Tran, et al.Review of chemical models and applications in Geant4-DNA: Report from the ESA BioRad III Project, Medical physics, (2024).

9. Vlastou E, Diamantopoulos S, Efstathopoulos EP, Monte Carlo studies in Gold Nanoparticles enhanced radiotherapy: The impact of modelled parameters in dose enhancement, *Physica Medica*, 2020, 80: 57-64.

10. Shin WG, Lee D, Jung JW, Kim CH. Geant4-DNA simulation of the pre-chemical stage of water radiolysis and its impact on initial radiochemical yields. Physica Medica. 2021; 88:86-90.

11.Incerti, S., et al. *Review of Geant4-DNA applications for micro and nanoscale simulations. Physica Medica, 2018, 45, 150-166.

12. Tamborino G, et al. Modeling Early Radiation DNA Damage Occurring During 177Lu-DOTATATE Radionuclide Therapy. Journal of Nuclear Medicine. 2022;63(5):761-769.

13. Kyriakou I, Incerti S, Francis Z. Influence of track structure and condensed history physics models of Geant4 to nanoscale electron transport in liquid water. Physica Medica. 2019; 58:149-154.

14. Lazarakis P, Incerti S, Ivanchenko VN, Kyriakou I, Emfietzoglou D, Corde S, et al. Investigation of track structure and condensed history physics models for applications in radiation dosimetry on a micro and nano scale in Geant4. Biomedical Physics & Engineering Express 2018.

15. Chatzipapas KP, Tran NH, Dordevic M, et al. Simulation of DNA damage using Geant4-DNA: an overview of the "molecularDNA" example application. Precision Radiation Oncology. 2023.

16. Pater P, Seuntjens J, El Naqa I, Bernal MA. On the consistency of Monte Carlo track structure DNA damage simulations. Medical Physics. 2014;41(12):121708.

17. Byrne HL, Gholami Y, Kuncic Z, Impact of fluorescence emission from gold atoms on surrounding biological tissue - implications for nanoparticle radio-enhancement, Physics in Medicine & Biology, 2017, 62(8): 3097-3110.

18. Fois GR, et al. Monte Carlo simulations of microdosimetry and radiolytic species production at long time post proton irradiation using GATE and Geant4-DNA. Medical Physics. 2024;51(10):7500-7510.

19. Okada S, et al. Quantitative estimation of track segment yields of water radiolysis species under heavy ions around Bragg peak energies using Geant4-DNA. Scientific Reports volume 11, Article number: 1524 (2021) 2021.

20. Chappuis F, et al. Modeling of scavenging systems in water radiolysis with Geant4-DNA. Physica Medica. 2023; 108:102549.

21. Yoon E, et al. Verification of Geant4-DNA step-by-step-reaction-diffusion master equation model for long-term radiolysis simulation. Physica Medica. 2025; 133:104983.

22. Runze Zhou et al, *Novel Implications of Nanoparticle-Enhanced Radiotherapy and Brachytherapy: Z-Effect and Tumor Hypoxia. J Metabolites, 2022 Oct 5;12(10):943.

23. J Naoki D-Kondo, et al. Effect of FLASH dose-rate and oxygen concentration in the production of H2O2 in cellular-like media versus water: a Monte Carlo track-structure study. Physics in Medicine and Biology. 2025;70(2):025014.

24.Jie Liu, et al. Synergistic cerium oxide nanozymes: targeting DNA damage and alleviating tumor hypoxia for improved NSCLC radiotherapy efficiency. Journal of Nanobiotechnology 22, 25 (2024).

25.Sun, H., Cai, H., Xu, C. et al. AGuIX nanoparticles enhance ionizing radiation-induced ferroptosis on tumor cells by targeting the NRF2-GPX4 signaling pathway, Journal of Nanobiotechnology 20, 449 (2022).

26. Koger B, Kirkby C. Dosimetric effects of polyethylene glycol surface coatings on gold nanoparticle radiosensitization. Physics in Medicine and Biology. 2017;62(21):8455-8469.

27.Gao, H., Sun, L., Ni, D. *et al.* Regulating electron transportation by tungsten oxide nanocapacitors for enhanced radiation therapy, Journal of Nanobiotechnology 21, 205 (2023). https://doi.org/10.1186/s12951-023-01962-8

28. Bian J, et al. GEANT4-DNA simulation of temperature-dependent and pH-dependent yields of chemical radiolytic species. Physics in Medicine and Biology. 2023;68(12).

29.Yan Luo, Radiobiological perspective on metrics for quantifying dose enhancement effects of High-Z nanoparticles, Biomedical Nanotechnology, Volume 7 – 2025.

30. Lindsey A. Bennie1, Jie Feng1, Christo, Formulating RALA/Au nanocomplexes to enhance nanoparticle internalisation efficiency, sensitising prostate tumour models to radiation treatment, Journal of Nanobiotechnology, (2021) 19:279

Supplementary Files

This is a list of supplementary files associated with this preprint. Click to download.

- BetaElectronAppendix.docx